# The interseismic velocity field of the Central Apennine from a dense GPS network

**Galvani A.[1], Anzidei M.[1], Devoti R.[1], Esposito A.[1], Pietrantonio G.[1], Pisani A. R.[1], Riguzzi F.[1], Serpelloni E.[2]**

[1] Istituto Nazionale di Geofisica e Vulcanologia, Centro Nazionale Terremoti, Via di Vigna Murata, 605 – 00143 Rome, Italy – www.ingv.it

[2] Istituto Nazionale di Geofisica e Vulcanologia, Centro Nazionale Terremoti, Via Donato Creti,12 - 40128 Bologna, Italy – www.bo.ingv.it

Alessandro Galvani – Istituto Nazionale di Geofisica e Vulcanologia, Centro Nazionale Terremoti, Via di Vigna Murata, 605 – Rome, Italy – www.ingv.it

+39-06-51860225

alessandro.galvani@ingv.it

**Abstract**

Since 1999 we have repeatedly surveyed the Central Apennines by a dense survey style geodetic network, the Central Apennine Geodetic Network (CAGeoNet), consisting of 123 benchmarks distributed over an area of ~180 x 130 km extend, from the Tyrrhenian to the Adriatic coasts with an average inter-site distance of 3-5 km. The network is located across the main seismogenic structures of the region, capable to generate destructive earthquakes. Here, we show the horizontal GPS velocity field of both the CAGeoNet and continuous GPS (CGPS) stations in this region, estimated from the position time series in the time span 1999-2007. We have analyzed the data using both the Bernese and the Gamit software, rigorously combining the two solutions to obtain a validated result. Then, we have analyzed the strain rate field, which shows a region of extension located along the axis of the Apennines chain, with values ranging from 2 to $66 \cdot 10^{-9}$ $yr^{-1}$ and a relative minimum of about $20 \cdot 10^{-9}$ $yr^{-1}$ located in the L'Aquila basin area. Our velocity field represents an improved estimation of the ongoing elastic inter-seismic deformation of central Apennines in particular of the L'Aquila earthquake of April 6$^{th}$, 2009 area.

**Key words:** Central Apennines, GPS velocity field, solutions combination, GPS surveys

## Introduction

According to current views, the Apennines chain is an arc–shaped, NE verging belt, characterized by a complex pattern of thrust and folds and normal faults related to two superimposed tectonic phases: an upper Miocene - lower Pleistocene compressional phase, forming NW–SE trending thrust and folds, and the subsequent Quaternary extensional phase, forming NW–SE trending normal faults responsible for the formation of large intramontane basins, filled by Plio–Quaternary continental sediments (i.e. L'Aquila, Rieti, Terni, Fucino and Sulmona basins) (Galadini & Messina, 1994; Galadini & Galli, 2000) (Fig. 1). Some authors explain the change of the tectonic regime as caused by the flexural retreat, through a roll back mechanism, of the lithospheric Adriatic plate dipping below the Apennines (Reutter et al., 1980; Boccaletti et al., 1982; Malinverno and Ryan, 1986; Royden et al., 1987; Patacca et al., 1990; Doglioni, 1991; Doglioni et al., 1994; Frepoli e Amato 1997; Basili & Barba, 2007). Other authors ascribe the change of the tectonic regime as caused by the NE motion, relative to Eurasia, of the Adriatic microplate around a rotation pole located in NW Italy (Anderson & Jackson, 1987; Calais et al., 2002; D'Agostino et al., 2005; D'Agostino et al., 2008). At present, geodetic data show that extensional deformation in the central Apennines is occurring along a narrow belt 30–40 km wide (Hunstad et al, 2003; Serpelloni et al., 2005; Devoti et al., 2008; Devoti et al., 2011), near the areas where the strongest historical (intensity $\geq$ XI) and instrumental earthquakes occurred (Boschi et al., 1998; Selvaggi, 1998) (Fig.1). Starting from 1999 a dense survey-mode GPS network (CAGeoNet) consisting of 123 benchmarks with an average inter-site distance of 3-5 km, now surrounded by continuously operating GPS stations (Fig.2), was designed and installed in the central Apennines (Anzidei et al., 2005; Anzidei et al., 2008) across the main active faults, as evidenced by geological and seismological data (Valensise & Pantosti, 2001; Galadini & Galli, 2000). The high GPS stations density and the quality of the data collected, provide new insights about the present-day deformation of this seismically active area, and gives information useful for seismic hazard assessments.

It has been shown that the combination of independent geodetic solutions, obtained with different GPS-processing software (Avallone et al., 2010; Devoti et al., 2012) allows to minimize eventual systematic errors and to validate the final velocity solutions. In this

work, we estimate the interseismic strain-rates from the combination of independent solutions obtained with the Bernese and Gamit softwares, thus investigating the geodetic deformation of the interseismic cycle of the Umbria-Marche Apennines (UMA) and Lazio–Abruzzo Apennines (LAA).

**The CAGeoNet and GPS campaigns**

The CAGeoNet network has been repeatedly measured during the time span 1999-2007. Surveys were planned taking into account the network grid, the number of stations to be measured simultaneously (up to 11) and the time required to move receivers through the network. Consistently with the logistics, measurements have been carried out approximately in the same period of the year to minimize possible biases due to seasonal variations. Each station was occupied for an average observation window of 48 h, for at least three survey sessions per station, with a sampling rate of 30 s.

Here we discuss the interseismic deformation field resulting from the analysis of velocities obtained from a sub-set of 55 CaGeoNet stations in the time-interval 1999-2007.

**Data processing and combination procedure**

The analyzed data set (Fig. 2) consists of GPS data collected on survey style benchmarks (the CAGeoNet benchmarks) and continuous data provided by the CGPS networks located in the Central Apennine region. The CGPS stations belonging to different GPS networks: IGS (http://igscb.jpl.nasa.gov), RING (Avallone et al., 2010), ASI (Vespe et al., 2000), Leica Geosystems (ItalPos network), the Regione Abruzzo and the Universities of Perugia and L'Aquila.

The GPS data cover the period from 1999 to 2007, and are arranged into several clusters, each one sharing common fiducial CGPS stations used as anchor stations in the subsequent combination. Each cluster has been independently processed, then combined by a least squares combination into a single daily solution. The GPS observations have been processed using both the Bernese 5.0 (Beutler et al., 2007) and Gamit 10.34 software (Herring et al., 2006).

The BERNESE processing is based on the BPE procedure, following the standard analysis for regional networks. We solve for daily stations coordinates together with hourly

troposphere parameters, using the a priori DRY NIELL troposphere model and estimating the corrections by the WET NIELL mapping function. Ionosphere was neither estimated nor modelled since we used the L3 (ionosphere–free) linear combination of L1 and L2. The a priori GPS orbits and Earth Orientation Parameters were fixed to the precise IGS products. We applied the ocean-loading model FES2004 and used the International GNSS Service (IGS) absolute antenna phase-center corrections. The daily solutions were obtained in a loosely constrained reference frame, i.e. all the a priori stations coordinates were left free to 10 m apriori sigma.

The GAMIT processing follows the standard procedures for the analysis of regional networks (e.g., McClucsky et al., 2000; Serpelloni et al., 2006), applying loose constraints to the geodetic parameters. The GAMIT software uses double-differenced, ionosphere-free linear combinations of the L1 and L2 phase observations, to generate weighted least square solutions for each daily session (Schaffrin & Bock, 1988; Dong & Bock, 1989). An automatic cleaning algorithm (Herring et al., 2006) is applied to post-fit residuals, in order to repair cycle slips and to remove outliers. The observation weights vary with elevation angle and are derived individually for each station from the scatter of post-fit residuals obtained in a preliminary GAMIT solution. The effect of solid-earth tides, polar motion and oceanic loading are taken into account according to the IERS/IGS standard 2003 model (McCarthy and Petit, 2004). We apply the ocean-loading model FES2004 and use the IGS absolute antenna phase-center correction table to model the effective receiver and satellites antennas phase-centers. We use orbits provided by the Scrips Orbit Permanent Array Center (SOPAC). Estimated parameters for each daily solution include the 3D cartesian coordinates for each station, the 6 orbital elements for each satellite, Earth Orientation Parameters (pole position and rate and UT1 rate) and integer phase ambiguities, applying loosely constraints (~10 m) to the apriori parameters. We also estimate hourly piecewise-linear atmospheric zenith delays at each station to correct the poorly modelled troposphere, and 3 east-west and north-south atmospheric gradients per day, to account for azimuth asymmetry; the associated error covariance matrix is also computed and saved in SINEX format.

Both the analysis procedures (BERNESE and GAMIT) produce daily loosely constrained solutions, i.e. free from any a priori reference frame datum. Coordinates and the complete associated covariance matrices were saved in SINEX format.

The time series of the two solutions were then obtained applying minimal inner constraints and a 4-parameter Helmert transformation to obtain coordinates and errors expressed in the IGS05 reference frame (the IGS realization of the ITRF2005 reference frame). Then, we obtained a velocity field for each solution estimating a linear drift (velocity), annual sinusoid and occasional offsets due to changes in the stations equipment from each time series.

**Combined GPS velocity field**

The two independent velocity solutions were combined in a unique velocity solution using a linear least squares combination approach. The normal matrix is formed from the two independent velocity solutions and then inverted to estimate the unified velocity field of the entire network. Since usually the covariance matrix is known apart from a constant multiplier, we estimate also a solution scale factor together with the combined velocity solution. This ensures that the individual $\chi^2$ of each velocity solution are equally balanced (individual solutions do not prevail in the combination process) and the total $\chi^2$ is close to unity (realistic errors). The combined solution represents a weighted velocity average taking into account the correlation matrices of the two solutions. The differences between the combined and the individual solutions have low mean values and comparable standard deviations (Fig. 3). The values reported in Figure 3 show how the combined solution is placed between the BERNESE and GAMIT solutions and does not give priority to any individual solution. The BERNESE solution is slightly more noisy in the east velocity component while the GAMIT solution is slightly more noisy in the north velocity component. The comparison between BERNESE and GAMIT solutions shows residuals whose average are -0.2 mm $yr^{-1}$ (Ve component) and 0.3 mm $yr^{-1}$ (Vn component) and dispersion values (at $1\sigma$ level) of 0.7 mm $yr^{-1}$ and 0.9 mm $yr^{-1}$ in Ve and Vn, respectively. The differences are comparable with the averaged sigma values computed for the permanent stations used in the individual solutions ($\sigma_E$ = 0.14 mm; $\sigma_N$ = 0.23 mm), highlighting how the solutions are compatible. We have made a statistical screening

between the combined solution with respect to each single solution (BERNESE and GAMIT) and the single solutions with respect to each other, both on permanent and non-permanent stations, comparing the differences obtained between the average values of Ve and Vn. Stations exhibiting differences greater than the respective 2σ values were discarded.

The combined velocity field with respect to an Eurasian-fixed reference frame is shown in Figure 4. The velocity components and their uncertainties are reported in Table 1. The Eurasia plate has been fixed minimizing the horizontal velocities of 24 stations located in the stable part of the plate. The selection of Eurasian stations is statistically inferred using a $\chi^2$ test-statistic to select the subset of stations defining the stable plate (Noquet et al., 2001) starting from the triad WSTR, WTZR and ZIMM stations in ITRF2005. The estimated Euler pole and rotation rate for Eurasia plate are at 55.85°N, 95.72°W and 0.266° ± 0.003° $Myr^{-1}$ respectively.

The geodetic strain rate has been evaluated by a distance-weighted approach, computed using all stations on a regularly spaced grid applying the weighting algorithm developed by Shen et al. (1996). The contribution of each station velocity to the strain-rate computed on a given node, is down weighted with the function $W= \exp(-d^2/\alpha^2)$, where $d$ is the distance between each node and the stations and α is the smoothing distance parameter. The algorithm selects the optimal α-value from a given *apriori* interval, depending on the spatial distribution of the GPS sites, consequently strain-rate maps are obtained with spatially variable α.

The second invariant rate has been obtained by interpolating the velocity horizontal components on a 0.1°x0.1° regular grid. The smoothing factor down-weights the velocities in the range from 20 to 100 km, according to the network density (Fig. 6).

**Results**

The combined horizontal velocity field, expressed with respect to a fixed Eurasian plate, (Fig. 4) shows i) a good coherence between velocities estimated from CAGeoNet (red arrows) and CGPS stations (blue arrows), ii) two different and characteristic main velocity patterns; a NNW oriented trend on the Apennine-Tyrrhenian sector and a NNE oriented trend on the Apennine-Adriatic sector. A gradual clockwise velocity rotation is clearly

186 evident from W to E, where velocities are initially NNW oriented and rotate towards NNE
187 increasing their values (0.9–5.2 mm $yr^{-1}$). This pattern shows an anomaly in the L'Aquila
188 basin where the vectors are turned ~ NS directed, normal to the main tectonic structures of
189 Gran Sasso Range (Fig. 4).
190 To better evidence the velocity gradients across the central Apennines chain, we have
191 represented the velocity field with respect to a fixed Tyrrhenian coast (Fig. 5) and then
192 projected the velocities along two profiles ENE – WSW oriented, crossing the studied area.
193 The two profiles are parallel to the average direction of the velocity vectors and
194 approximately normal to the main fault systems. Profile 1) is located across the Umbria-
195 Marche Apennines sector (UMA), profile 2) is located across the Lazio–Abruzzi Apennines
196 (LAA) sector. The projections contain all the velocities within the distance of 40 km
197 (profiles 1), and 30 km (profile 2). To highlight the velocity gradient, we use a moving-
198 average filter, with a 40 km window (grey line in Fig. 5). The net extension rates across the
199 two cross sections are the same, ~2.5 mm $yr^{-1}$, but spreading over different distances.
200 Profile 1 shows a velocity variation concentrated in an narrow strip of ~ 60 km, with
201 maximum step of 1.5 mm $yr^{-1}$ occurring in about 30 Km, on the western flank of the chain
202 with a strain rate of about $50 \cdot 10^{-9}$ $yr^{-1}$. Profile 2 shows a more irregular velocity variation,
203 with a negative (i.e., shortening component) gradient roughly in correspondence of
204 L'Aquila basin (between 120 and 150 km, Figure 5, profile 2), and developing along larger
205 distance (~ 100 km.) with respect to profile 1 with a lower strain rate of about $20 \cdot 10^{-9}$ $yr^{-1}$.
206 The predominantly extensional deformation is mainly oriented NE–SW, ranging from $2 \pm 11 \cdot 10^{-9}$ $yr^{-1}$ to $66 \pm 19 \cdot 10^{-9}$ $yr^{-1}$ (Fig. 6).
208 In Umbria-Marche Apennines (UMA) the extensional deformation is distributed in a
209 relatively wide area, coinciding with the culmination of topographic relief. The distribution
210 of extension area becomes to be narrower and shifted toward SW, crossing the Ancona-
211 Anzio Line (AAL), with slightly lower extension rates.
212 These estimations are in general agreement with those obtained by previous geodetic and
213 geologic data for this area. From geologic data, which include both interseismic and
214 coseismic deformations, Galadini & Galli (2000) obtain, across the main active fault sets
215 recognized in the area, an extension rate from 0.7 to 1.6 mm $yr^{-1}$; Faure Walker et. al (2010)
216 using fault slip vectors, calculate strain rates, averaged over 15 kyrs, of $12 \cdot 10^{-9}$ $yr^{-1}$ and an

extension rate of 1mm $yr^{-1}$ over a 160x80 km area, consistent with a strain rate $\leq 38 \cdot 10^{-9}$ $yr^{-1}$ estimated in 5x80 km boxes crossing the strike of the central Apennines. From geodetic data, Serpelloni et al. (2005) indicate $31 \cdot 10^{-9}$ $yr^{-1}$, while D'Agostino et al (2008) show a second invariant band parallel to the chain, with values > $50 \cdot 10^{-9}$ $yr^{-1}$. Devoti et al. (2008, 2011) estimate extension rate of $50 \cdot 10^{-9}$ $yr^{-1}$. Our results disagree with those obtained by Pesci et al. (2010), on a CAGeoNet network sub-set. They found a NE shortening in correspondence of the Umbria-Marche Apennines, a NW shortening in the Liri Valley and a wide area characterized by NE extension in the eastern portion of the Lazio–Abruzzo Apennines.

A relative minimum of the strain second invariant ($20 \cdot \pm$ 11 $10^{-9}$ $yr^{-1}$ ) is evidenced in the area where the April 6$^{th}$, 2009 earthquake occurred (Fig. 6). This value is congruent, with the extension rate of $10 \pm 4 \cdot 10^{-9}$ $yr^{-1}$ obtained by Doglioni et al (2011) using only CGPS stations. The L'Aquila basin area, that experienced in the past large historical earthquakes, has been characterized by a relative low instrumental seismicity in the last 30 years (1978 – 2008) (Fig. 1).

Viscoelastic earthquake cycle models (e.g., Lundgren et al. 2009) show that velocity gradients across faults may depend on crustal rheology and the fault stage in the earthquake cycle. The relative low strain-rate value observed across the L'Aquila basin by the dense CaGeoNet network, could be interpreted, in this light, as due to its position in a later stage of the earthquake cycle (e.g., Doglioni et al., 2011).

## Conclusion

We processed more than 100 GPS stations in central Italy, combining both permanent and survey-style networks. Thanks to the high number of stations and their short inter-distances (3–5 km), our data set provides the most detailed view of the sub-regional deformation field of this area. To validate our results, we have used two different strategies and GPS data processing software. The two independent velocity solutions strongly agree (horizontal WRMS 1.1 mm $yr^{-1}$ ) and their combination represents the best compromise of the available solution. Since relevant seismicity did not occur in the Lazio-Abruzzo Apennine during the considered time span (Fig. 1), we can assume that the observed velocity field is purely inter-seismic, thus describing the regional and elastic deformation field before the 2008–

2009 L'Aquila seismic sequence, culminated with the April 6$^{th}$ 2009 $M_w$ 6 earthquake. The horizontal velocities of our non-permanent stations often show large uncertainties (average values of about 1 and 1.5 mm yr$^{-1}$ in Ve, Vn respectively), nevertheless they are consistent with the CGPS velocity field estimated in this area.

The horizontal velocities and the strain rate results are consistent with the major tectonic features of the central Apennines showing a NE-SW extensional deformation style.

We estimate a differential velocity of about 2.5 mm yr$^{-1}$ across the Apennines, recognizing two different extensional deformation patterns; the Umbria–Marche Apennines sector shows a gradual velocity increase from W to E, while the Lazio–Abruzzo Apennines sector shows an irregular velocity increase characterized by two small steps. A moderate velocity decreasing is located in corrispondence of the L'Aquila basin.. The total strain rate values range from 2 to 66·10$^{-9}$ yr$^{-1}$. A relative minimum of about 20·10$^{-9}$ yr$^{-1}$ is located in the area of the L'Aquila basin, thus emphasizing the possible role of strain rate pattern in seismic hazard assessment. Shen et al. 2007 observed that, regions with higher strain concentration are more prone to be the source of future earthquakes, thus the relative minimum observed in the L'Aquila basin should not necessarily represent a decrease of the probability of earthquake occurrence, but could be interpreted as due to the locked part of the fault in the brittle upper crust approaching the end of the seismic cycle (Doglioni et al., 2011; Lundgren et al., 2009).

Despite the high concentration of the stations in the L'Aquila area, more near field studies are necessary to solve the behaviour of the crust in this region, still keeping open the debate.

**Acknowledgments**

We are thankful to Angelo Massucci and Sergio Del Mese for the CAGeoNet field work and data storage.

## References


Anderson, H. and J. Jackson (1987). Active tectonics of the Adriatic region, Geophys. J. R. Astron. Soc. 91, 937-983.

Anzidei, M., A. Galvani, A. Esposito, P. Cristofoletti, A. Pesci, P. Baldi, G. Casula, N. Cenni, F. Loddo and E. Serpelloni (2003). The Central Apennines Geodetic Network (CA-Geonet): description and preliminary results, XXVIII European Geophysical Society General Assembly, Geophys. Res.: Abstr, vol 5, abstr EAE03-A-05288.

Anzidei, M., P. Baldi, A. Pesci, A. Esposito, A. Galvani, F. Loddo, P. Cristofoletti, A. Massucci and S. Del Mese (2005). Geodetic deformation across the Central Apennines from GPS data in the time span 1999-2003, Annals of Geophysics, 48 (2), 259-271.

Anzidei, M., P. Baldi and E. Serpelloni (2008). The coseismic ground deformations of the 1997 Umbria-Marche earthquakes: a lesson for the development of new GPS networks, Annals of Geophysics, 51, 27-43.

Anzidei, M., E. Boschi, V. Cannelli, R. Devoti, A. Esposito, A. Galvani, D. Melini, G. Pietrantonio, F. Riguzzi, V. Sepe, and E. Serpelloni, (2009). Coseismic deformation of the destructive April 6, 2009 L'Aquila earthquake (central Italy) from GPS data, Geophys. Res. Lett., 36, L17307, doi:10.1029/2009GL039145.

Avallone, A., G. Selvaggi, E. D'Anastasio, N. D'Agostino, G. Pietrantonio, F.Riguzzi, E. Serpelloni, M. Anzidei, G. Casula, G. Cecere, C. D'Ambrosio, P. De Martino, R. Devoti, L. Falco, M. Mattia, M. Rossi, F. Obrizzo, U. Tammaro, and L. Zarrilli (2010). The RING network: improvements to a GPS velocity field in the central Mediterranean, Annals of Geophysics, 53 (2), doi: 10.4401/ag-4549.

Basili, R. and S. Barba (2007). Migration and shortening rates in the northern apennines, Italy: implications for seismic hazard, Terra Nova 19, 462-468, doi: 10.1111/J.1365-3121.2007.00772.x 2007.

Beutler, G. et al. (2007). Bernese GPS Software, edited by R. Dach, U. Hugentobler, P. Fridez and M. Meindl (Eds), Astronomical Institute, University of Bern ( January 2007).

Boccaletti, M., C. Conedera, P. Dainelli and P. Gocev (1982). The recent (Miocene–Quaternary) regmatic system of the western Mediterranean region, J. Pet. Geol, 5, 31-49.

Boschi, E., E. Guidoboni, G. Ferrari, and G. Valensise (1998). I terremoti dell'Appenino Umbro-Marchigiano (area sud orientale dal 99 a. C. al 1984), ING-SGA, compositori, Bologna, Italy.

Calais, E., J.M. Noquet, F. Jouanne, and M. Tardy (2002). Current strain regime in the western Alps from continuos Global Positioning System measurements, 1996-2001, Geology 7, 651-654.

D'Agostino, N., D. Cheloni, S. Mantenuto, G. Selvaggi, A. Michelini, and D. Zuliani (2005). Strain accumulation in the southern Alps (NE Italy) and deformation at the northeastern boundary of Adria observed by CGPS measurements, Geophys. Res. Lett. 32, L19306, doi: 10.1029/2005GL024266.

D'Agostino, N. A. Avallone, D. Cheloni, E. D'Anastasio, S. Mantenuto, and G. Selvaggi, (2008). Active tectonics of the Adriatic region from GPS and earthquake slip vectors, J. Geophys. Res. 113, B12413, doi: 10.1029/2008JB005860.

Devoti, R., F. Riguzzi, M. Cuffaro and C. Doglioni (2008). New GPS constraints on the kinematics of the Apennines subduction, Earth Planet Sci. Lett. 273, 163-174.

Devoti, R., A. Esposito, G. Pietrantonio, A.R. Pisani, and F. Riguzzi (2011). Evidence of large scale deformation patterns from GPS data in the Italian subduction boundary, Earth and Planet. Sci. Lett. 311, 230-241, doi: 10.1016/J.epsl.2011.09.034.

337 Devoti, R., E. Flammini, G. Pietrantonio, F. Riguzzi and E. Serpelloni (2012). Toward a
338 dense Italian GPS velocity field: data analysis strategies and quality assessment, N. Sneeuw
339 et al. (eds.), *VII Hotine-Marussi Symposium on Mathematical Geodesy*, International
340 Association of Geodesy Symposia 137, DOI 10.1007/978-3-642-22078-4 51, Springer-
341 Verlag Berlin Heidelberg.
342
343 Doglioni, C. (1991). A proposal for Kinematic modeling of W-dipping subduction-possible
344 applications to the Tyrrhenian-Apennines system, Terra Nova 3, 423-434.
345
346 Doglioni, C., F. Mongelli and P. Pieri (1994). The Puglia uplift (SE Italy): an anomaly in
347 the foreland of the Apenninic subduction due to buckling of a thick continental lithosphere,
348 Tectonics 13, 1309-1321.
349
350 Doglioni, C., S. Barba, E. Carminati and F. Riguzzi (2011). Role of the brittle-ductile
351 transition on fault activation, Phys. Earth Planet. Inter. 184, 160-171, doi:
352 10.1016/j.pepi.2010.11.005.
353
354 Dong, D. and R.W. Bock (1989). GPS network analysis with phase ambiguity resolution
355 applied to crustal deformation studies in California, J. Geophys. Res. 94, 3949-3966.
356
357 Faure Walker, J.P., G.P. Roberts, P.R. Sammonds and P. Cowie (2010). Comparison of
358 earthquake strains over $10^2$ and $10^4$ year timescales: Insights into variability in the seismic
359 cycle in the central Apennines, Italy, J. Geophys. Res, 115, B10418, doi:
360 10.1029/2009JB006462
361
362 Frepoli, A. and A. Amato (1997). Contemporaneous extension and compression in the
363 Northern Apennines from earthquake fault-plane solutions, Geophys. J. Int., 129, 268-388.
364
365 Galadini, F. and P. Messina (1994). Plio-Quaternary tectonic of the Fucino basin and
366 sorroundings areas (central Italy), Giorn. Geol., 56, 73-99.
367

368 Galadini, F. and P. Galli (2000). Active tectonics in the Central Apennines (Italy) – input
369 data for seismic hazard assessment, Nat. Hazard, 22, 225-270.
370
371 Herring, T., R.W. King, and S. McClusky (2006). GAMIT Reference Manual, Release
372 10.3. Department of Earth, Atmospheric, and Planetary Sciences, Massachussetts Institute
373 of Technology. (http://www-gpsg.mit.edu/~simon/gtgk/).
374
375 Lundgren, P., Eric A. Hetland, L. Zhen, and Eric J: Fielding (2009). Southern San Andreas-
376 San Jacinto fault system slip rates estimated from earthquake cycle models constrained by
377 GPS and interferometric syntetic aperture radar observation, J. Geophys. Res., 114,
378 B02403, doi:10.1029/2008JB005996.
379
380 Malinverno, A. and W.B.F. Ryan (1986). Extension in the Tyrrhenian sea and shortening in
381 the Apennines as result of arc migration driven by sinking of the lithosphere, Tectonics 5,
382 227-245.
383
384 McCarthy, D. D. and G. Petit (2004). IERS Conventions (2003). IERS Technical Note 32,
385 Verlag des Budesamts fur Kartographie und Geodasie, Frankfurt, paperback, ISBN 3-
386 89888-884-3 (print version).
387
388 McClusky, S., S. Balassanian, A. Barka, C. Demir, S. Ergintav, I. Georgiev, O. Gurkan, M.
389 Hamburger, K. Hurst, H. Kahle, K. Kastens, G. Kekelidze, R. King, V. Kotzev,O. Lenk, S.
390 Mahmoud, A. Mishin, M. Nadariya, A. Ouzounis, D. Paradissis, Y. Peter, M. Prilepin, R.
391 Reilinger, I. Sanli, H. Seeger, A. Tealeb, M.N. Toksöz and G. Veis (2000). Global
392 Positioning system constraints on plate kinematics and dynamics in the eastern
393 Mediterranean and Caucasus, J. Geophys. Res., 105, 5695-5719.
394
395 Noquet, J.M., E. Calais, Z. Altamimi, P. Sillard, and C. Boucher (2001). Intraplate
396 deformation in western Europe deduced from analysis of the International Terrestrial
397 Reference Frame 1997 (ITRF97) velocity field, J. Geophys. Res. 106 (B6), 11.239-11.257.
398

399 Patacca, E., R. Sartori and P. Scandone (1990). Tyrrhenian basin and Apenninic arcs;
400 kinematic relations since Late Tortonian times, Mem. Soc. Geol. It. 45, 425-451.
401
402 Pesci, A., G. Teza, G. Casula, N. Cenni, and F. Loddo (2010). Non-permanent GPS data for
403 regional-scale kinematics: reliable deformation rate before the 6 April, 2009, earthquake in
404 the L'Aquila area, Annals of Geophysics, 53 (2), doi: 10.4401/ag-4740.
405
406 Reutter, K.J., P. Gieseand, and H. Closs (1980). Lithospheric split in the descending plate:
407 observations from the Northern Apennines, Tectonophysics 64, T1-T9.
408
409 Royden, L., E. Patacca, and P. Scandone (1987). Segmentation and configuration of
410 subducted lithosphere in Italy: an important control on thrust–belt and foredeep-basin
411 evolution, Geology 15, 714-717.
412
413 Schaffrin, B. and Y. Bock, (1988). A unified scheme for processing GPS phase
414 observations, Bulletin Geodesique 62, 142–160.
415
416 Selvaggi, G. (1998). Spatial distribution of horizontal seismic strain in the Apennines from
417 historical earthquakes, Ann. Geof. 41 (2), 241-251.
418
419 Selvaggi, G., RING Working Group (2006). La Rete Integrata nazionale GPS (RING)
420 dell'INGV: una infrastruttura aperta per la ricerca scientifica, X Conferenza nazionale
421 dell'ASITA Bolzano (Italy), 14-17 novembre.
422
423 Serpelloni, E., M. Anzidei, P. Baldi, G. Casula and A. Galvani (2005). Crustal velocity and
424 strain-rate fields in Italy and surrounding regions: new results from the analysis of
425 permanent and non-permanent GPS networks, Geophys. J. Int., 161(3), 861-880.
426 doi:10.1111/j.1365-246X.2005.02618.x.
427
428 Serpelloni, E., G. Casula, A. Galvani, M. Anzidei, and P. Baldi, (2006). Data analysis of
429 permanent GPS networks in Italy and surrounding regions: application of a distributed

processing approach, Annals of Geophysics, 49, 897-928.

Shen, Z-K., D.D. Jackson and B.X. Ge (1996). Crustal deformation across and beyond the Los Angeles basin from geodetic measurements, J. Geophys. Res., 101 (B12), 27957-27980.

Shen, Z-K., D.D. Jackson and Y.Y. Kagan (2007). Implication of Geodetic Strain Rate for future earthquakes, with a five-year forecast of M5 earthquakes in southern California, Seis Res. Lett., 78 (1), 116-120.

Valensise, G. and D. Pantosti (editors) (2001). Database of potential sources for earthquakes larger than M 5.5 in Italy, Ann. Geof. suppl. Vol. 4484.

Vespe, F., G. Bianco, M. Fermi, C. Ferraro, A. Nardi and C. Sciarretta (2000). The Italian GPS fiducial network: services and products, J. Geodyn., 30, 327-336.

# Tables

| station | lat | lon | East mm/yr | sigE mm/yr | North mm/yr | sigN mm/yr | smaj-ax mm | smin-ax mm | azim |
|---|---|---|---|---|---|---|---|---|---|
| ACCU | 42.696 | 13.241 | 0.5 | 1.0 | 3.2 | 1.7 | 2.5 | 1.5 | -173 |
| AQUI | 42.368 | 13.350 | 0.5 | 0.1 | 2.9 | 0.1 | 0.1 | 0.1 | 90 |
| ARAG | 42.411 | 13.459 | -0.2 | 0.6 | 3.3 | 1.1 | 1.7 | 0.9 | -171 |
| ASCO | 42.822 | 13.637 | 1.7 | 0.3 | 2.3 | 0.3 | 0.5 | 0.4 | 176 |
| ATRA | 42.551 | 14.007 | 0.8 | 0.2 | 2.6 | 0.3 | 0.5 | 0.3 | 9 |
| BANO | 42.337 | 13.582 | 0.2 | 1.1 | 2.4 | 1.9 | 3.0 | 1.6 | -171 |
| BLRA | 41.810 | 13.560 | -0.4 | 0.2 | 3.3 | 0.4 | 0.6 | 0.3 | -168 |
| BORB | 42.511 | 13.162 | 0.3 | 1.0 | 1.5 | 1.4 | 2.1 | 1.4 | -179 |
| BSPI | 42.306 | 13.650 | 1.0 | 1.3 | 1.4 | 2.0 | 3.0 | 1.9 | -171 |
| BSSO | 41.546 | 14.594 | 0.8 | 0.1 | 3.6 | 0.2 | 0.3 | 0.2 | -174 |
| CADO | 42.293 | 13.483 | -0.3 | 0.6 | 2.3 | 0.9 | 1.3 | 0.9 | -176 |
| CAME | 43.112 | 13.124 | 2.1 | 0.0 | 3.6 | 0.1 | 0.1 | 0.1 | 179 |
| CASB | 42.390 | 12.849 | -1.1 | 0.9 | 1.7 | 1.5 | 2.3 | 1.4 | 179 |
| CDRA | 42.368 | 13.720 | -0.5 | 0.2 | 3.9 | 0.3 | 0.5 | 0.3 | -170 |
| CEPP | 42.530 | 12.855 | -0.8 | 0.6 | 1.2 | 0.9 | 1.4 | 0.9 | -169 |
| CERT | 41.949 | 12.982 | -1.1 | 0.2 | 1.8 | 0.2 | 0.4 | 0.2 | -173 |
| CESI | 43.005 | 12.905 | 0.3 | 0.3 | 3.6 | 0.4 | 0.6 | 0.4 | -171 |
| CHNO | 42.654 | 13.062 | -0.2 | 1.3 | 4.4 | 2.0 | 3.1 | 1.9 | -174 |
| CINC | 42.008 | 13.405 | -0.3 | 1.4 | 1.2 | 2.3 | 3.5 | 2.0 | -170 |
| CORT | 42.827 | 12.987 | 2.0 | 1.3 | 4.9 | 2.1 | 3.2 | 2.0 | -173 |
| CPAG | 42.501 | 13.288 | -0.2 | 0.6 | 2.8 | 0.9 | 1.3 | 1.0 | -166 |
| CROG | 42.586 | 13.485 | 0.5 | 0.8 | 2.1 | 1.2 | 1.9 | 1.3 | -177 |
| CTOS | 42.564 | 13.359 | 1.8 | 1.1 | 3.4 | 1.8 | 2.7 | 1.7 | -176 |
| CVAL | 41.984 | 13.811 | 0.0 | 1.4 | 3.9 | 2.4 | 3.7 | 2.0 | -171 |
| CVSE | 42.131 | 13.745 | 0.1 | 1.4 | 4.1 | 2.2 | 3.4 | 2.1 | -173 |
| FCLM | 42.111 | 13.459 | -0.4 | 1.2 | 2.3 | 2.0 | 3.1 | 1.8 | -171 |
| FRCA | 42.059 | 13.678 | 1.0 | 1.3 | 2.2 | 2.1 | 3.2 | 1.9 | -172 |
| FRRA | 42.418 | 14.292 | 0.8 | 0.2 | 3.1 | 0.3 | 0.5 | 0.3 | -172 |
| INGP | 42.383 | 13.316 | 0.8 | 0.1 | 2.9 | 0.2 | 0.3 | 0.2 | -175 |
| INGR | 41.828 | 12.515 | -0.7 | 0.1 | 1.8 | 0.1 | 0.2 | 0.1 | -172 |
| LARI | 41.810 | 14.922 | 1.5 | 0.4 | 4.2 | 0.4 | 0.7 | 0.6 | 172 |
| LNSS | 42.603 | 13.040 | 1.1 | 0.2 | 2.1 | 0.3 | 0.4 | 0.2 | 7 |
| M0SE | 41.893 | 12.493 | -0.5 | 0.2 | 2.0 | 0.3 | 0.4 | 0.3 | 177 |
| MAON | 42.428 | 11.131 | -0.6 | 0.1 | 0.8 | 0.2 | 0.3 | 0.2 | -175 |
| MICI | 42.460 | 13.054 | -0.2 | 0.9 | 2.0 | 1.4 | 2.1 | 1.4 | -171 |
| MLNN | 41.822 | 13.705 | -1.1 | 1.6 | 2.6 | 2.7 | 4.1 | 2.4 | -169 |
| MMAR | 42.102 | 13.363 | -1.2 | 0.7 | 2.5 | 1.2 | 1.9 | 1.0 | -173 |
| MRPN | 41.886 | 13.685 | -1.0 | 1.7 | 2.0 | 2.7 | 4.2 | 2.5 | -173 |
| MRRA | 42.885 | 13.916 | 1.4 | 0.2 | 3.1 | 0.3 | 0.5 | 0.3 | -172 |
| MSAN | 42.761 | 13.154 | 1.3 | 0.9 | 2.9 | 1.2 | 1.9 | 1.3 | -170 |
| MSNI | 42.527 | 13.363 | 1.1 | 1.0 | 2.4 | 1.6 | 2.5 | 1.4 | -173 |
| OCRA | 42.050 | 13.039 | -1.2 | 0.4 | 2.1 | 0.6 | 0.9 | 0.5 | 9 |
| PBRA | 42.124 | 14.229 | 0.1 | 0.2 | 3.8 | 0.3 | 0.5 | 0.3 | -171 |
| PERU | 43.111 | 12.394 | 0.6 | 0.4 | 1.9 | 0.5 | 0.8 | 0.6 | 165 |
| PESC | 42.024 | 13.667 | 0.1 | 1.1 | 2.1 | 1.7 | 2.6 | 1.6 | -170 |
| POCA | 42.571 | 13.326 | 0.7 | 0.9 | 4.3 | 1.2 | 1.8 | 1.3 | -177 |
| POGB | 42.515 | 12.873 | 0.3 | 0.8 | 1.4 | 1.3 | 2.1 | 1.2 | 9 |

| | | | | | | | | | |
|---|---|---|---|---|---|---|---|---|---|
| PPEZ | 42.183 | 13.426 | 0.7 | 1.2 | 2.5 | 2.0 | 3.1 | 1.7 | -175 |
| PSCA | 42.128 | 13.125 | -1.2 | 1.1 | 2.3 | 1.8 | 2.7 | 1.7 | -174 |
| PSMA | 42.127 | 13.581 | 0.8 | 1.1 | 2.1 | 1.7 | 2.6 | 1.7 | -175 |
| PSTE | 42.428 | 11.120 | -0.1 | 0.7 | 1.0 | 0.8 | 1.2 | 1.1 | 164 |
| REFO | 42.956 | 12.704 | 0.8 | 0.1 | 2.2 | 0.2 | 0.2 | 0.2 | -173 |
| RENO | 42.793 | 13.093 | 1.0 | 0.1 | 2.3 | 0.1 | 0.2 | 0.1 | -171 |
| REPI | 42.952 | 12.002 | -0.1 | 0.1 | 2.1 | 0.2 | 0.2 | 0.1 | -173 |
| RETO | 42.782 | 12.407 | -0.2 | 0.1 | 1.8 | 0.1 | 0.2 | 0.1 | -173 |
| RIET | 42.408 | 12.857 | 0.1 | 0.5 | 0.0 | 0.6 | 1.0 | 0.8 | 177 |
| RIFP | 42.763 | 13.176 | 0.9 | 0.9 | 3.6 | 1.4 | 2.1 | 1.4 | -174 |
| RNI2 | 41.703 | 14.152 | 0.3 | 0.1 | 3.1 | 0.2 | 0.4 | 0.2 | 7 |
| ROCA | 42.328 | 13.697 | 0.5 | 1.0 | 3.0 | 1.6 | 2.5 | 1.5 | -173 |
| ROFA | 42.397 | 13.541 | -0.1 | 0.7 | 1.3 | 1.1 | 1.6 | 1.0 | -174 |
| ROIO | 42.327 | 13.386 | 0.1 | 0.4 | 3.6 | 0.5 | 0.8 | 0.6 | 176 |
| RSTO | 42.658 | 14.001 | 1.2 | 0.0 | 3.3 | 0.1 | 0.1 | 0.1 | -177 |
| S260 | 42.601 | 13.257 | 0.8 | 1.2 | 2.8 | 1.8 | 2.8 | 1.8 | -170 |
| SCIN | 42.434 | 13.559 | 0.0 | 0.6 | 3.4 | 1.1 | 1.7 | 0.9 | -171 |
| SCRA | 42.268 | 14.002 | 0.3 | 0.2 | 3.0 | 0.3 | 0.4 | 0.3 | -171 |
| SECI | 42.148 | 13.670 | 0.9 | 1.2 | 4.2 | 1.8 | 2.8 | 1.8 | -174 |
| SELL | 42.369 | 13.180 | 1.1 | 0.7 | 3.1 | 0.9 | 1.3 | 1.0 | 176 |
| SI01 | 42.964 | 11.901 | -0.2 | 0.6 | 2.2 | 0.7 | 1.1 | 0.9 | 173 |
| SIER | 41.925 | 13.668 | -0.1 | 1.1 | 1.9 | 1.9 | 2.8 | 1.7 | -173 |
| SLLI | 42.727 | 13.121 | 0.6 | 1.6 | 3.0 | 2.4 | 3.6 | 2.3 | -174 |
| SLUC | 42.567 | 13.261 | 1.0 | 1.5 | 3.9 | 2.1 | 3.3 | 2.2 | 5 |
| SMCO | 42.393 | 13.271 | -0.3 | 0.6 | 3.7 | 0.9 | 1.4 | 0.9 | -179 |
| SMPQ | 42.055 | 13.394 | 0.3 | 0.8 | 2.0 | 1.4 | 2.1 | 1.2 | -173 |
| SMRA | 42.048 | 13.924 | 0.7 | 0.2 | 3.0 | 0.3 | 0.4 | 0.3 | -170 |
| SORB | 42.082 | 13.317 | -0.6 | 1.2 | 2.2 | 1.9 | 2.9 | 1.8 | -174 |
| SS83 | 41.842 | 13.780 | -0.4 | 1.7 | 2.0 | 2.8 | 4.2 | 2.5 | -173 |
| SSMF | 42.131 | 13.221 | 0.2 | 1.0 | 1.7 | 1.6 | 2.5 | 1.6 | -177 |
| SSTS | 42.360 | 13.651 | 0.8 | 1.1 | 1.8 | 2.1 | 3.1 | 1.7 | -172 |
| TARI | 42.459 | 13.276 | 0.8 | 1.2 | 2.0 | 1.9 | 2.9 | 1.8 | -170 |
| TNER | 42.237 | 13.532 | -0.5 | 1.1 | 1.2 | 2.0 | 3.0 | 1.7 | -173 |
| TODI | 42.781 | 12.408 | -0.6 | 0.6 | 2.2 | 0.7 | 1.1 | 0.9 | 155 |
| TOLF | 42.064 | 12.000 | -0.9 | 0.1 | 1.8 | 0.2 | 0.3 | 0.2 | -174 |
| TRAS | 41.954 | 13.543 | 0.1 | 1.1 | 3.2 | 1.6 | 2.5 | 1.6 | 11 |
| TRIV | 41.767 | 14.550 | 0.7 | 0.2 | 3.6 | 0.3 | 0.5 | 0.3 | -171 |
| TRMT | 42.096 | 13.201 | -1.2 | 0.7 | 2.8 | 1.2 | 1.9 | 1.0 | -172 |
| TRNE | 42.441 | 13.198 | 0.7 | 0.8 | 2.7 | 1.3 | 2.0 | 1.2 | -173 |
| UNOV | 42.716 | 12.113 | -0.1 | 0.2 | 1.7 | 0.3 | 0.5 | 0.3 | -172 |
| UNPG | 43.119 | 12.356 | -0.4 | 0.1 | 1.9 | 0.2 | 0.2 | 0.2 | 179 |
| UNTR | 42.559 | 12.674 | 0.7 | 0.1 | 1.7 | 0.2 | 0.2 | 0.2 | 179 |
| VCRA | 42.735 | 13.498 | 1.3 | 0.2 | 3.0 | 0.4 | 0.6 | 0.3 | -174 |
| VITE | 42.418 | 12.119 | -0.9 | 0.7 | 1.9 | 0.8 | 1.2 | 1.0 | 177 |
| VNRE | 42.001 | 13.646 | 0.5 | 0.9 | 1.9 | 1.6 | 2.4 | 1.4 | -173 |
| VRCE | 42.039 | 13.240 | 0.1 | 0.8 | 2.5 | 1.3 | 2.0 | 1.1 | -174 |
| VTRA | 42.110 | 14.708 | 0.5 | 0.2 | 2.9 | 0.3 | 0.4 | 0.3 | -171 |
| VVLO | 41.870 | 13.623 | -0.2 | 0.1 | 2.6 | 0.2 | 0.3 | 0.2 | -174 |

**Table 1**

448 **Figure caption**

449 **Fig. 1**: Geological settings of the Umbria-Marche Apennines (UMA) Lazio-Abruzzo
450 Apennines (LAA): main fault systems and intramontane basins, Terni basin (TB), Rieti
451 basin (RB), L'Aquila basin (AB), Fucino basin (FB), Sulmona basin (SB) are reported with
452 instrumental (1978-2008) and historical (I>10) (CPTI04)
453 (http://emidius.mi.ingv.it/CPTI04) seismicity distribution.

454 **Fig. 2** :The CAGeoNet (triangles) and the CGPS stations (blue dots) used in our analyses.

455 **Fig. 3**: The residuals between the combined and the individual (BERNESE, GAMIT)
456 solutions.

457 **Fig. 4**: GPS combined velocity field estimated for the time span 1999-2007 with respect to
458 the Eurasian plate. CAGeoNet GPS velocities are shown with red arrows; continuous GPS
459 velocities are shown with blue arrows.

460 **Fig. 5**: The velocity projection along the transect directions 1a–1b / 2a–2b. The projection
461 involved vertices at a distance of 20 and 15 km in both perpendicular directions along the
462 transect directions for the profile 1a -1b and 2a – 2b respectively.

463 **Fig. 6**: The second invariant estimated on a 0.1°x0.1° regular grid according to the
464 algorithm of Shen et al. (1996).

465

466 **Table caption**

467 Table1. Velocity field (mm $yr^{-1}$) of the CAGeoNet and of the surrounding CGPS stations
468 used in the analysis. In the columns are reported site name, site coordinates, velocities E
469 and N (both in mm $yr^{-1}$), sigma E and sigma N (both in mm $yr^{-1}$) and error ellipses with
470 azimuth.

471

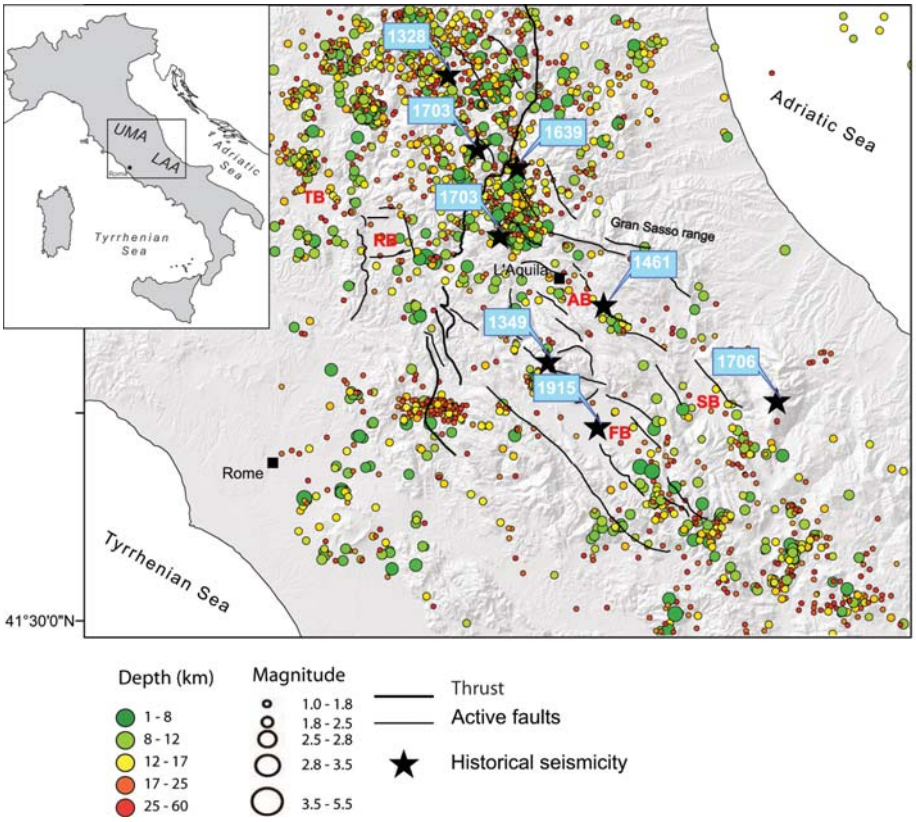


472

473

474 **Figure 1**

475

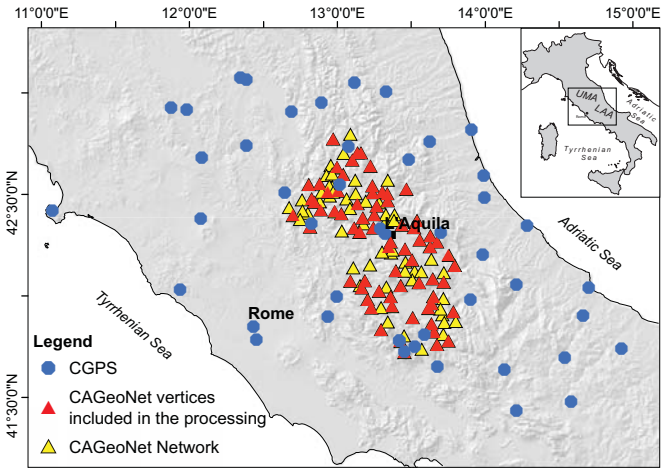


476

477

478 **Figure 2**

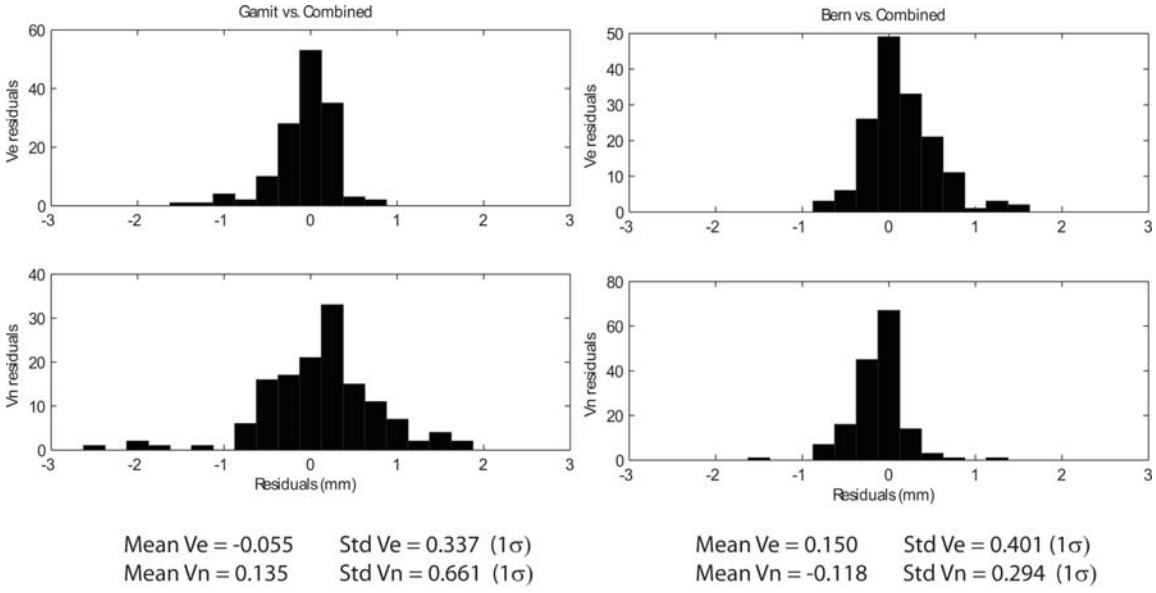


479

480

481 **Figure 3**

482

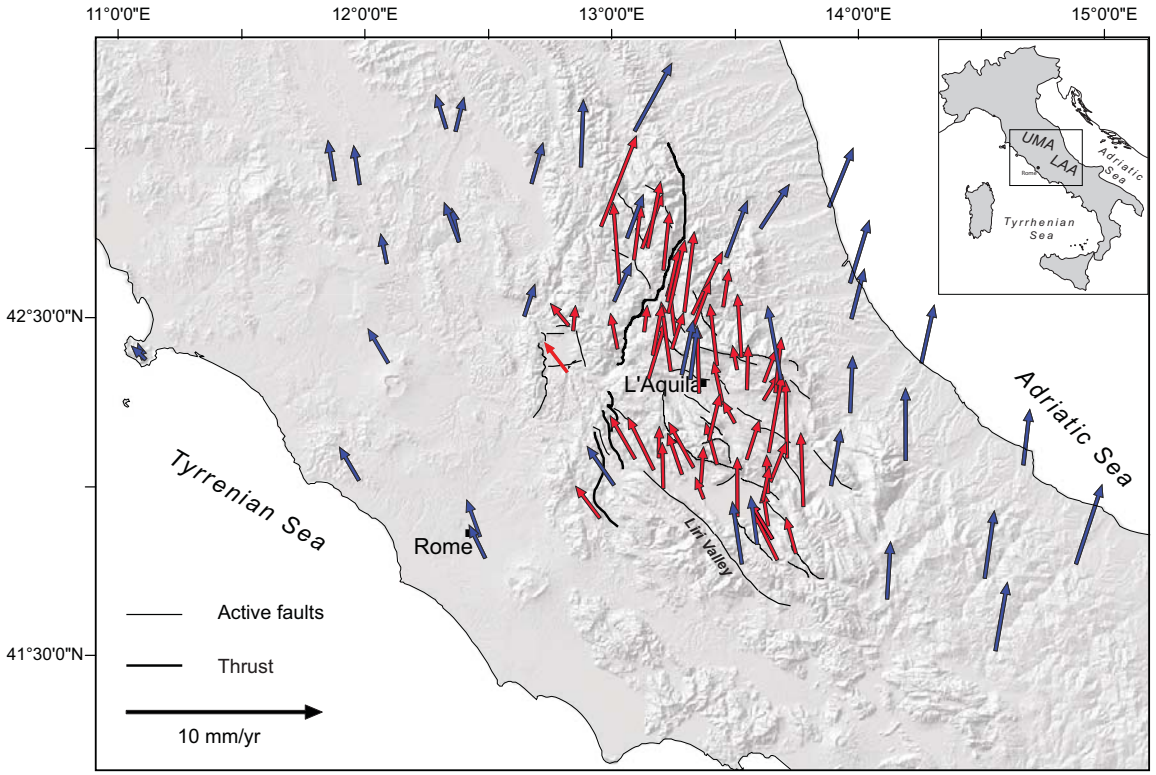


483

**Figure 4**

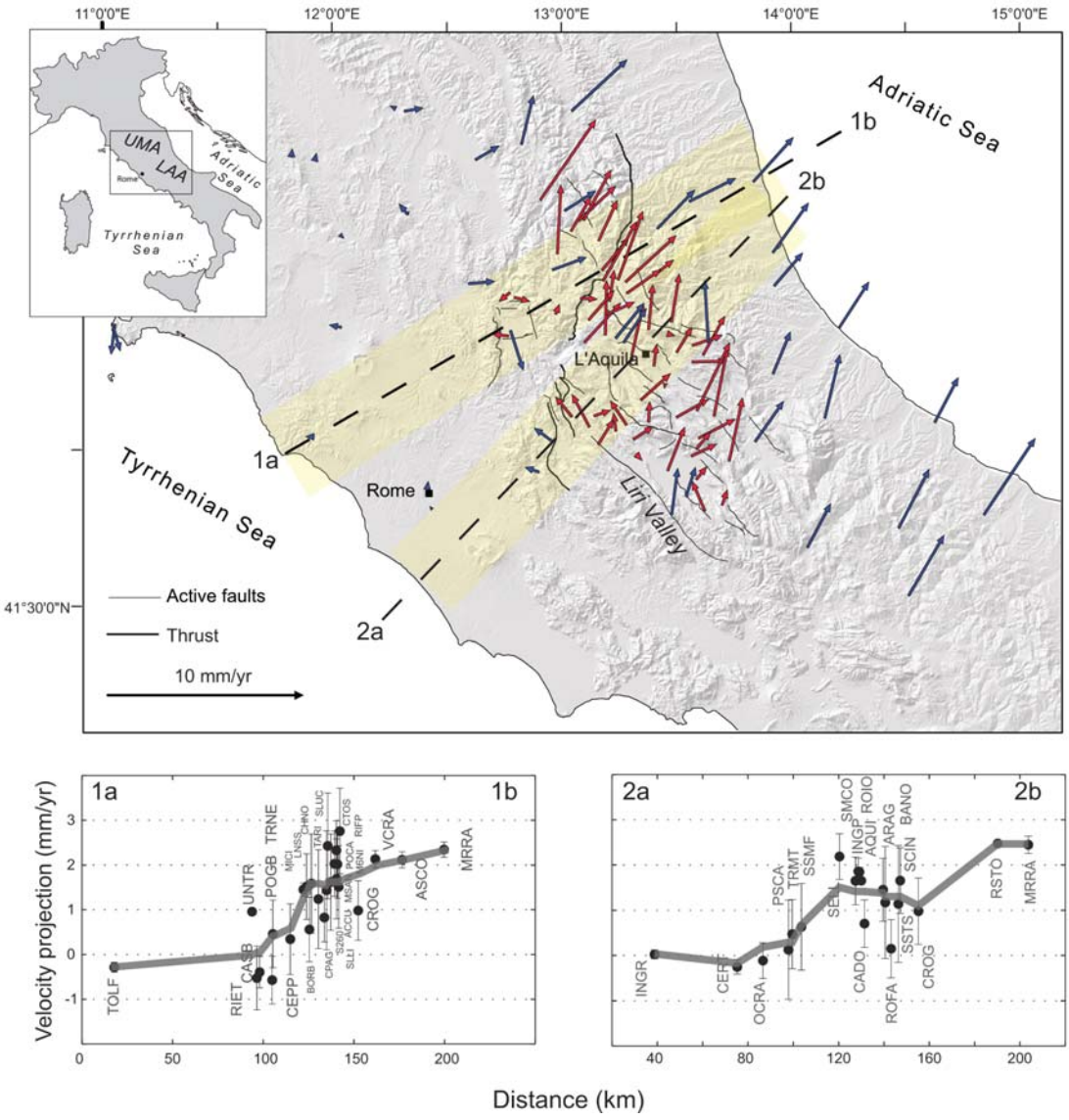


**Figure 5**

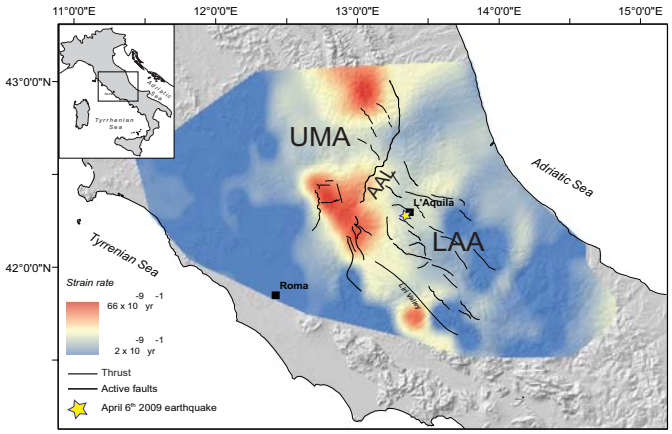


489

490

491 **Figure 6**